energies

MDPI

Article

Robust Bilevel Optimal Dispatch of Park Integrated Energy System Considering Renewable Energy Uncertainty

Puming Wang [1], Liqin Zheng [2], Tianyi Diao [3], Shengquan Huang [1] and Xiaoqing Bai [1,*]

[1] Guangxi Key Laboratory of Power System Optimization and Energy Technology, School of Electrical Engineering, Guangxi University, Nanning 530004, China; 2112392094@st.gxu.edu.cn (P.W.); 2212392044@st.gxu.edu.cn (S.H.)
[2] State Grid Xiamen Electric Power Supply Company, Xiamen 361004, China; zhengliqin@st.gxu.edu.cn
[3] State Grid Liaocheng Power Supply Company, Liaocheng 252000, China; dty19960817521@st.gxu.edu.cn
* Correspondence: baixq@gxu.edu.cn

Abstract: This paper focuses on optimizing the park integrated energy system (PIES) operation, and a robust bilevel optimal dispatch is proposed. Firstly, the robust uncertainty set is constructed based on the K-means++ algorithm to solve the uncertainty of renewable energy sources output in PIES. Then, the bi-level dispatch model is proposed, with the operator as the leader and consumers as the follower. The upper model establishes an electricity-heat-gas integrated energy network, and the lower model considers the demand response of consumers. Optimizing the pricing strategies of energy sources to determine the output of each energy conversion equipment and the demand response plan. Moreover, analyzing the decision-making process of the robust bi-level model and the solution method is given. Finally, case studies show that the proposed dispatch model can increase operator profits and reduce consumers' energy costs. The in-sample and out-of-sample simulations demonstrate that the proposed ellipsoid uncertainty set possesses high compactness, good robustness, and low conservatism.

Keywords: K-means++; robust bilevel optimization; multi-energy flow model; demand response

check for updates

Citation: Wang, P.; Zheng, L.; Diao, T.; Huang, S.; Bai, X. Robust Bilevel Optimal Dispatch of Park Integrated Energy System Considering Renewable Energy Uncertainty. *Energies* **2023**, *16*, 7302. https://doi.org/10.3390/en16217302

Received: 4 October 2023
Revised: 23 October 2023
Accepted: 25 October 2023
Published: 27 October 2023

Copyright: © 2023 by the authors. Licensee MDPI, Basel, Switzerland. This article is an open access article distributed under the terms and conditions of the Creative Commons Attribution (CC BY) license (https://creativecommons.org/licenses/by/4.0/).

1. Introduction

1.1. Motivation and Incitement

As energy depletion and environmental pollution become increasingly serious, our traditional energy distribution model can no longer meet the demands of modern society. To address this, we must promote the development of clean energy industries and build a safe and efficient new energy system [1,2]. Against this background, the Park Integrated Energy System (PIES) [3] coordinates and optimizes multiple energy sources, making full use of renewable energy [4] while promoting the complementary advantages of different energy sources and satisfying the diverse energy needs of consumers in a specific region [5]. However, in the process of multi-energy interaction, due to the involvement of different stakeholders, the interaction between them is relatively complex, which will bring serious challenges to the operation and regulation of PIES. Moreover, with the increasing share of renewable energy, the intermittence and randomness of its output also have a greater impact on the reliability of the system. Therefore, it is of great significance to study the operation regulation of PIES under the consideration of renewable energy uncertainty and complex interest relations.

1.2. Literature Review

In recent years, a growing focus has been on addressing the uncertainty of renewable energy sources [6]. To tackle this issue, researchers have utilized robust optimization, a mathematical approach that involves constructing uncertainty sets to obtain a worst-case scenario [7]. These sets can include the box set, ellipsoidal set, polyhedral set, and the

union of multiple sets [8,9]. Currently, researchers have improved or combined conventional uncertainty sets. With the development of artificial intelligence technology, a new method based on data-driven uncertainty sets has been proposed for robust optimization, which can effectively reduce the conservativeness of conventional robust optimization. Reference [10] used machine learning techniques to construct uncertainty sets through data-driven active learning from available data. Reference [11] used the improved k-means method to find typical days and extreme days in the historical optimization data set to solve the randomness of system source and load. This demonstrates that clustering techniques have been recognized in analyzing load or renewable energy generation data. In view of the uncertainty of renewable energy output in PIES, the above research did not endeavor to employ the improved K-means algorithm as the data foundation for the construction of uncertainty sets. However, the data-driven technology, which is grounded in clustering algorithms, provides a novel idea for mitigating the detrimental influence of indeterminate parameters on the operation optimization of PIES.

In general, exploring the operation optimization of PIES is essential to study the coupling characteristics of multiple energy sources, the non-stationarity of renewable energy output, and the energy flow distribution characteristics of integrated energy networks [12]. In PIES, two stakeholders, the operator and consumers, exchange various forms of energy, such as electricity, cold, and heat, for mutual benefit [13,14]. The complex interest interaction and the autonomous behavior of consumers can bring enormous difficulties to the entire system's operation. On the other hand, considering the consumer as a more dynamic entity, they can also positively impact scheduling through proper guidance, thereby making the decision-making entities in PIES more diverse [15]. Demand response, a scheme that guides consumers to cooperate with operation optimization, reflects its value and role in many literatures. Reference [16] achieved cut peaks and filled valleys through the cooperation of energy storage equipment and comprehensive demand response. By exploring essential techniques and models for implementing integrated demand response, reference [17] evaluated and optimized these strategies. Reference [18] guided users' energy consumption habits through multi-type demand response strategies to participate in the coordinated operation of integrated energy systems. The above literature fully reflects the value of demand response in improving economic performance, flexibility, and reliability. However, the demand response models in the literature above were predominantly used as the interest constraints for users to participate in the operation optimization of the integrated energy system while overlooking the game interaction process.

Optimization emphasizes the coordinated and efficient operation of multiple energy sources on the operator side. It is generally believed that precise modeling of energy devices and energy networks will have a significant impact on the economy of PIES. For example, in the power flow calculation of the power network, network loss is an essential and unavoidable part. Similarly, for the coupling between different energy sources, when conducting a theoretical analysis of PIES, it is necessary to establish an accurate, multi-energy flow model for power, heat, and gas networks [19,20]. Reference [21] proposed a generalized quasi-dynamic model and decomposition iterative solution method for dynamic processes, network topology, and variable quality flow of the electric-thermal coupling system considering both the power and thermal networks. Reference [22] carried out linear modeling based on the physical properties of the gas network and power system. In order to reduce the computational burden of the subsequent interaction process, the complex multi-energy flow model on the supply side should also be appropriately linearized [23]. Despite providing a comprehensive overview of the modeling process of the integrated energy network and calculation methodologies for integrated energy flow, the above literature has rarely involved the issue of user demand response and the interaction with the energy network game simultaneously.

In the study of the game interaction between different stakeholders, the bilevel model is most suitable to describe this process. When conducting energy transactions, the operator guides consumers to demand response by rationally allocating and scheduling various

energy sources [24]. When the bi-level optimization model involves data uncertainty [25], combined with the robust optimization method described above, it forms a robust bi-level optimization problem. In that case, it will cause serious solution difficulties. In reference [26], the author developed a bi-level hybrid robust-stochastic framework to consider the randomness of renewable energy in the game interaction between microgrid aggregators and market operators. Setting aside the differences between the above literature and the research background of this paper, it is of forward-looking significance for the solution of the robust bilevel model. Due to the maturity of research in single-level optimization, similar approaches can be applied to address the robust bilevel optimization problem [27].

1.3. Contribution

This paper focuses on optimizing the park integrated energy system (PIES) operation, and a robust bilevel optimal dispatch is proposed. Compared with the existing research work, the innovations and contributions of this paper are as follows:

Based on the K-means++ clustering algorithm, a data-driven robust optimization method for constructing ellipsoidal uncertainty sets is proposed. It clarifies the possible range of uncertain parameters and reduces the conservatism of the solution. Then, we establish a bi-level dispatch model, with the operator as the leader and the consumers as the follower. The upper model employs an electricity-heat-gas integrated energy network with renewable energy, designing the concrete topology of the park and calculating the integrated energy flow. The lower model considers the demand response of consumers by optimizing the pricing strategies of energy sources to determine the output of each energy conversion equipment and the demand response plan. After analyzing the decision-making process of bi-level optimization, a specific solution process is given. Case studies are conducted to verify the effectiveness of the proposed method.

2. Robust Bilevel Optimization Model

2.1. Robust Optimization Model

2.1.1. K-Means++ Clustering Technique

As the proportion of renewable energy in the PIES increases, flexibility improves, and various random factors intertwine, making the economic dispatch of the system complex. This paper preprocessed the historical data of wind and solar using the K-means++ clustering algorithm. The initial cluster center is randomly selected by dividing the time series data into disjoint hourly sections and determining a clustering number. The K-means++ clustering algorithm [28,29] improves the traditional K-means clustering algorithm, aiming to maximize the distance between the initial cluster centers. The process is as follows: firstly, the initial cluster center c_i is randomly selected from a sample point r_i in the dimensionality-reduced data matrix $R = [r_1 r_2 \ldots r_{n'}]_{n' \times n}$, with n' representing the reduced dimensionality and r being an n'-dimensional vector. Secondly, the shortest Euclidean distance $d_j = \| r_j - c_i \|_2^2$ between the clustering vector r_j of the jth cluster and c_i is computed. Thirdly, the probability p_j of r_j and is calculated, and the next cluster center is the one with the highest probability p_{jm}:

$$p_j = \frac{d_j}{\sum_{k=1}^{m} d_k} \tag{1}$$

Then, repeat the above steps until all cluster centers are identified. Finally, the clustering results are available with the K-means++ algorithm. Repeat the above steps until the average error between the cluster centers and the predicted values is less than 0.05%, indicating the termination of clustering. Selecting n samples from around each cluster and substituting them into the ellipsoidal set. To be clear the K-Means++ clustering algorithm does not directly obtain the predicted value but clarifies the possible range of uncertain parameters through it.

2.1.2. The Ellipsoidal Uncertainty Set

The actual values of wind and solar power are composed of fluctuation quantity and predicted values, and an ellipsoidal set describes the uncertainty of the fluctuation quantity. The robust model is formulated as follows:

$$P_i^{WT} = \zeta_1 + \overline{P_i^{WT}} \tag{2}$$

$$P_i^{PV} = \zeta_2 + \overline{P_i^{PV}} \tag{3}$$

$$\Omega_1 = \left\{ \zeta_1 \in R^{n_{\zeta_1}} : \zeta_1^\top \sum \zeta_1 \leq 1 \right\} \tag{4}$$

$$\Omega_2 = \left\{ \zeta_2 \in R^{n_{\zeta_2}} : \zeta_2^\top \sum \zeta_2 \leq 1 \right\} \tag{5}$$

where $\overline{P_i^{WT}}$ and $\overline{P_i^{PV}}$ represent the predicted values of wind and solar power, respectively; P_i^{WT} and P_i^{PV} represent the actual values of wind and solar power, respectively; ζ_1 and ζ_2 describe the fluctuation of wind and solar power; Ω_1 and Ω_2 are the ellipsoidal sets constructed from the fluctuations of wind and solar power, respectively.

When defining Ω, the symbol Σ in the equation represents [9]:

$$\sum = Diag\ \sqrt{\sigma} \begin{bmatrix} 1 & \frac{1}{|n|} & \cdots & \frac{1}{|n|} \\ \frac{1}{|n|} & 1 & \cdots & \frac{1}{|n|} \\ \cdots & \cdots & \cdots & \cdots \\ \frac{1}{|n|} & \frac{1}{|n|} & \frac{1}{|n|} & 1 \end{bmatrix} Diag\ \sqrt{\sigma} \tag{6}$$

The variable σ is defined through the predicted wind and solar power values and the uncertainty. n represents the number of samples selected around each cluster center.

$$\sigma_{1,i} = \frac{1}{\left(W\overline{P_i^{WT}}\right)^2} \tag{7}$$

$$\sigma_{2,i} = \frac{1}{\left(W\overline{P_i^{PV}}\right)^2} \tag{8}$$

where W represents the uncertainty level, which can be adjusted from 0 to 1.

2.2. Leader Model

2.2.1. The Objective Function

The PIES operator establishes an objective function to maximize profits, represented by the difference between revenue and cost. Specifically, the operator's revenue from selling energy equals the cost of consumers buying energy and C_{OPE} represents the operating cost.

$$\max P_R = \sum_{e \in E} \sum_{t=1}^{T} [L_{e,R}(t) \cdot \gamma_e(t)] - C_{OPE} \tag{9}$$

$$C_{OPE} = \sum_{t=1}^{T} \left[P_{ele}^{in}(t)\varphi_{ele}(t) + S_i^{in}(t)\varphi_{gas}(t) + \left| \overline{P_i^{WT}}(t) - P_i^{WT}(t) \right| \cdot w_1 + \left| \overline{P_i^{PV}}(t) - P_i^{PV}(t) \right| \cdot w_2 \right] \tag{10}$$

where $E = \{ele, heat\}$ denotes the set of two types of energy used by consumers; $L_{e,R}(t)$ denotes the load after energy e participates in demand response at time t. $\gamma_e(t)$ represents the price of energy e at time t, which is established by the operator and published to consumers; $P_e^{in}(t)$ represents the power input in interactions with the external system

during time t; $L_i^{in}(t)$ represents the volume of natural gas input to the PIES during time t and $\varphi_e(t)$ represents the price of energy purchased from the external system by the PIES, which is established and published by the electricity and gas companies. w_1 and w_2, respectively, represent the unit penalty costs for wind and solar prediction errors.

2.2.2. Constraints

(1) Component model

To meet relevant policy requirements, corresponding energy storage devices are installed for renewable energy units according to 20% of their capacity. In addition, other energy-coupling components also include gas turbines, CHP, and boilers.

(a) Energy storage model

$$E_t = E_{t-\Delta t} + \eta^{ch} P_t^{ch} \cdot \Delta t - \eta^{dis} P_t^{dis} \cdot \Delta t \tag{11}$$

$$r_t^{ch} + r_t^{dis} \leq 1 \tag{12}$$

$$r^{ch} P_{\min}^{ch} \leq P_t^{ch} \leq r^{ch} P_{\max}^{ch} \tag{13}$$

$$r^{dis} P_{\min}^{dis} \leq P_t^{dis} \leq r^{dis} P_{\max}^{dis} \tag{14}$$

$$E_{\min} \leq E_t \leq E_{\max} \tag{15}$$

$$\sum_{t=1}^{T} \eta^{ch} P_t^{ch} = \sum_{t=1}^{T} \eta^{dis} P_t^{dis} \tag{16}$$

where $E_{t-\Delta t}$ and E_t represent the energy storage capacity at the previous and current time, respectively; P_t^{ch} and P_t^{dis} represent the charging and discharging power; η^{ch} and η^{dis} represent the charging and discharging efficiency. In the actual charging and discharging process, an inevitable loss will occur on the charging and discharging power, which this factor can represent. r_t^{ch} and r_t^{dis} represent the charging and discharging indicators, which are binary variables and are used to limit the charging and discharging activities to different periods. $P_{\max}^{ch}$, $P_{\min}^{ch}$, $P_{\max}^{dis}$ and $P_{\min}^{dis}$ represent the upper and lower limits of the charging and discharging power, respectively; $E_{\max}$ and $E_{\min}$ represent the upper and lower limits of energy storage capacity.

(b) Gas Turbine

The gas turbine is a device that converts natural gas into electrical energy and has the advantages of fast start-up and convenient scheduling. The mathematical model is as follows:

$$P_i^{GT} = \eta_{GT} H_g L_i^{GT} \tag{17}$$

$$0 \leq P_i^{GT} \leq P_{\max}^{GT} \tag{18}$$

where L_i^{GT} represents the natural gas flow consumed by the gas turbine; P_i^{GT} and $P_{\max}^{GT}$, respectively, represent the electrical power output and upper limit of the gas turbine; η_{GT} is the power generation efficiency of the gas turbine; H_g represents the natural gas calorific value.

(c) CHP

A combined heat and power (CHP) unit is a device that can convert natural gas into both electrical and thermal energy:

$$P_i^{CHP} = \eta_{CHP} H_g L_i^{CHP} \tag{19}$$

$$P_{\min}^{CHP} \le P_i^{CHP} \le P_{\max}^{CHP} \tag{20}$$

$$\Phi_i^{CHP} = z_{CHP} P_i^{CHP} \tag{21}$$

$$\Phi_{\min}^{CHP} \le \Phi_i^{CHP} \le \Phi_{\max}^{CHP} \tag{22}$$

where P_i^{CHP}, $P_{\max}^{CHP}$, and $P_{\min}^{CHP}$ respectively represent the electrical power output and its upper and lower limits of the CHP unit; Φ_i^{CHP}, $\Phi_{\max}^{CHP}$, $\Phi_{\max}^{CHP}$ and $\Phi_{\min}^{CHP}$ represent the heat power output and its upper and lower limits of the CHP unit respectively; η_{CHP} and z_{CHP} represent power generation efficiency and thermal-electricity ratio of the CHP unit; is the natural gas consumption of the CHP unit.

(d) Boiler

The boiler can convert natural gas into heat energy:

$$\Phi_i^{GB} = \eta_{GB} H_g L_i^{GB} \tag{23}$$

$$\Phi_{\min}^{GB} \le \Phi_i^{GB} \le \Phi_{\max}^{GB} \tag{24}$$

where L_{GB} is the natural gas consumption; Φ_i^{GB}, $\Phi_{\min}^{GB}$ and $\Phi_{\max}^{GB}$ represent the heat power output and its upper and lower limits; η_{GT} represents the thermal efficiency of the boiler.

(2) Multi-energy network model

(a) Power flow model

The optimal AC power flow constraints are expressed in the Second Order Cone Programming (SOCP) format [30].

$$P_i^G - P_i^d = G_{ii} c_{ii} + \sum_{\substack{j=1 \\ j \ne i}}^{k} \left[G_{ij} c_{ij} + B_{ij} s_{ij} \right] \tag{25}$$

$$Q_i^G - Q_i^d = -B_{ii} c_{ii} + \sum_{\substack{j=1 \\ j \ne i}}^{k} \left[B_{ij} c_{ij} + G_{ij} s_{ij} \right] \tag{26}$$

$$P_i^G = P_i^{WT} + P_i^{PV} + P_i^{dis} - P_i^{ch} + P_i^{CHP} + P_i^{GT} + P_i^{in} \tag{27}$$

$$\left(V_i^{\min}\right)^2 \le c_{ii} \le \left(V_i^{\max}\right)^2 \tag{28}$$

$$P_i^{G,\min} \le P_i^G \le P_i^{G,\max} \tag{29}$$

$$Q_i^{G,\min} \le Q_{i,t}^G \le Q_i^{G,\max} \tag{30}$$

$$\left(-G_{ij} c_{ii} + G_{ij} c_{ij} + B_{ij} s_{ij}\right)^2 + \left(B_{ij} c_{ii} - B_{ij} c_{ij} - G_{ij} s_{ij}\right)^2 \le \left(P_{ij}^{\max}\right)^2 \tag{31}$$

where P_i^G and P_i^d are the active power output of the source and the active power load of the node; Q_i^G and Q_i^d are the reactive power output of the source and the reactive power load of the node. $P_i^{G,\max}$ and $P_i^{G,\min}$ represent the upper and lower limits of the active power output of the source; $Q_i^{G,\max}$ and $Q_i^{G,\min}$ represent the upper and lower limits of the reactive power output; $V_i^{\max}$ and $V_i^{\min}$ represent the upper and lower limits of the node voltage. $P_{ij}^{\max}$ is the maximum power that the line $i-j$ can bear. G_{ij} and B_{ij} are the conductance and susceptance of line $i-j$.

c_{ii}, c_{jj} and s_{ij} are introduced node variables that satisfy the following constraints:

$$\begin{cases} c_{ij} = c_{ji} \\ s_{ij} = -s_{ji} \\ c_{ij}^2 + s_{ij}^2 + \leq c_{ii}c_{jj} \end{cases} \tag{32}$$

(b) Thermal network model

The thermal network constraints are as follows:

$$\begin{cases} \Phi_i^G = C_p m_{i,q}(T_{i,s} - T_{i,r}) \\ \Phi_i^d = C_p m_{i,q}(T_{i,s} - T_{i,o}) \end{cases} \tag{33}$$

$$\Phi_i^G = \Phi_i^{GB} + \Phi_i^{CHP} \tag{34}$$

$$T_{i,end} = (T_{i,start} - T_a)e^{-\frac{\lambda L}{C_p m}} + T_a \tag{35}$$

$$\left(\sum_{i=1}^{N} m_{i,out}\right) T_{i,out} = \sum_{i=1}^{N} (m_{i,in} T_{i,in}) \tag{36}$$

$$T_{s,\min} \leq T_{i,s} \leq T_{s,\max} \tag{37}$$

$$T_{o,\min} \leq T_{i,o} \leq T_{o,\max} \tag{38}$$

$$m_{q,\min} \leq m_{i,q} \leq m_{q,\max} \tag{39}$$

Φ_i^G and Φ_i^d are the thermal power output and thermal load power of node i; C_p is the specific heat capacity of water; T_s is the supply temperature of the node i; $T_{i,r}$ is the return temperature of the node i; T_o is the output temperature of the node i; T_{start} is the temperature at the beginning of the pipeline, and T_{end} is the temperature at the end of the pipeline; T_a is the ambient temperature, set to $T_a = 10\ ^\circ\mathrm{C}$; λ is the heat transfer coefficient, set to $\lambda = 0.2\ \mathrm{W} \cdot (\mathrm{m} \cdot \mathrm{K})^{-1}$; m_{in} is the flow rate of the pipeline flowing into the node, while m_{out} is the flow rate of the pipeline flowing out of the node; T_{in} is the temperature input at the end of the pipeline and T_{out} is the node output temperature; $T_{s,\max}$ and $T_{s,\min}$ represent the upper and lower limits of the node's supply water temperature, while $T_{o,\max}$ and $T_{o,\min}$ represent the upper and lower limits of the nodes' return water temperature; $m_{q,\max}$ and $m_{q,\min}$ represent the upper and lower limits of the pipeline flow.

For the sake of the nonlinearity of the temperature drop Equation (39), linearization is achieved through Taylor expansion:

$$T_{end} = (T_{start} - T_a)e^{-\frac{\lambda L}{C_p m}} + T_a \approx (T_{start} - T_a)\left(1 - \frac{\lambda L}{C_p m} + \frac{1}{2}\frac{\lambda^2 L^2}{C_p^2 m^2}\right) + T_a \tag{40}$$

(c) Natural gas pipeline network model

The natural gas pipeline network system model mainly includes the gas pipeline flow equations and the gas node flow balance equations.

$$\sum_{i=1}^{N} S_i^G = \sum_{i=1}^{N} \sum_{j=1}^{N_0} S_{ij}^G = \sum_{i=1}^{N} S_i^d \tag{41}$$

$$S_i^G = S_i^{CHP} + S_i^{GT} + S_i^{GB} \tag{42}$$

$$(U_i^t)^2 - (U_j^t)^2 = sign(S_{ij}^G) a_{ij} (S_{ij}^G)^2 \tag{43}$$

$$U_i^{\min} \le U_i^t \le U_i^{\max} \tag{44}$$

where $S_{i,t}^G$ is the gas flow rate at node i at time t; N is the number of nodes in the system; N_0 represents the set of other nodes connected to node i; $S_{ij,t}^G$ represents the gas flow rate between node i and j, $S_{ij}^{G,\max}$ represents the maximum gas transmission capacity of the natural gas pipeline between node i and j; $sign(\cdot)$ is the sign function. If the direction of natural gas flow is from node i to node j, then $sign(S_{ij}^G) = +1$, otherwise, $sign(S_{ij}^G) = -1$; a_{ij} depends on the physical characteristics of the pipeline and is an inherent parameter of the pipeline; U_i^t is the pressure at node i, $U_i^{\max}$ and $U_i^{\min}$ represent the upper and lower limits of the pipeline pressure at node i.

For the sake of the non-convexity of Equation (43), convexification of the equation as a mixed-integer second-order cone programming (MI-SOCP) problem is achieved by introducing variables $x_l = sign(S_{ij,t}^G)$ and $z_{li} = (U_i^t)^2 x_l$, $z_{lj} = (U_j^t)^2 x_l$:

$$x_l (U_i^{\min})^2 \le z_{li} \le x_l (U_i^{\max})^2 \tag{45}$$

$$-S_{ij}^{G,\max}(1 - x_l) \le S_{ij}^G \le x_l S_{ij}^{G,\max} \tag{46}$$

$$2z_{li} - 2z_{lj} + (U_j^t)^2 - (U_i^t)^2 \ge a_{ij} (S_{ij,t}^G)^2 \tag{47}$$

(3) Energy price constraints

From the perspective of time-of-use electricity price, while protecting consumer interests, the energy price announced by the operator cannot exceed the baseline price of energy; otherwise, consumers are more likely to purchase energy directly from the system's external sources. The baseline energy price is determined based on the PIES procurement price considering equipment depreciation. Additionally, the energy sales prices must be made overall constraints within a period.

$$\begin{cases} \gamma_{ele}(t) \le \gamma_{ele,B}(t) \\ \gamma_{heat}(t) \le \gamma_{heat,B}(t) \end{cases} \tag{48}$$

$$\begin{cases} \sum\limits_{t=1}^{T} \gamma_{ele}(t) \le T\overline{\gamma}_{ele.\max} \\ \sum\limits_{t=1}^{T} \gamma_{heat}(t) \le T\overline{\gamma}_{heat.\max} \end{cases} \tag{49}$$

$\gamma_{ele}(t)$ and $\gamma_{heat}(t)$ represent consumers' actual purchase prices of electricity and heat, while $\gamma_{ele,B}(t)$ and $\gamma_{heat,B}(t)$ are the baseline prices of electricity and heat. $\overline{\gamma}_{ele.\max}$ and $\overline{\gamma}_{heat.\max}$ represent the upper limits of the average electricity and heat sales prices.

2.3. Follower Model

2.3.1. The Objective Function

The objective function representing consumers' interests is maximizing comprehensive benefits U_{LA} [31].

$$\max U_{LA} = \sum_{t=1}^{T} \left\{ f_U(t) - \sum_{e \in E} [L_{e,R}(t) \cdot \gamma_e(t)] \right\} \tag{50}$$

Consumers respond to the operator's pricing signals by adjusting their energy demand while introducing a utility function that measures their satisfaction with their energy usage to safeguard their interests. From an economic perspective, the numerical values of the utility function have no practical significance. The essence of introducing it into the model is to serve as a metric for measuring economic benefits [32,33].

$$f_U(t) = \sum_{e \in E} \left[\alpha_e L_{e,R}(t) - \beta_e L_{e,R}^2(t) \right] \tag{51}$$

The equation, $f_U(t)$ represents the energy utility of the consumers; α_e and β_e are energy preference parameters, their practical meaning is similar to energy prices.

2.3.2. Constraints

(a) Electric load model

The electrical load is divided based on fixed loads and adjustable loads. During demand response, the load is shifted from the adjustable load while maintaining the fixed load as the baseline.

$$L_{ele,R}(t) = L_{BE}(t) + L_{ME}(t) \tag{52}$$

$$L_{ME,min} \le |L_{ME}(t)| \le L_{ME,max} \tag{53}$$

$$\sum_{t=1}^{T} L_{ele,R}(t) = \sum_{t=1}^{T} \sum_{i=1}^{N} P_i^d(t) \tag{54}$$

where $L_{ele,R}(t)$ represents the actual electrical load, $L_{BE}(t)$ is the fixed load, the duration of which is relatively certain to ensure consumers' normal living and working needs. $L_{ME}(t)$ represents the transferable power load, which is transferred by consumers based on the energy prices published by the operator. $L_{ME,max}$, $L_{ME,min}$ represent upper and lower limits of transferable power load; (54) indicates that the load remains balanced before and after demand response during one period.

(b) Heat load model

Similarly, the PIES also involves heat load, whose load composition is roughly the same as that of power load, including fixed heat load and reducible heat load, represented as:

$$L_{heat,R}(t) = L_{BH}(t) - L_{MH}(t) \tag{55}$$

$$L_{MH,min} \le |L_{MH}(t)| \le L_{MH,max} \tag{56}$$

$$\sum_{t=1}^{T} L_{heat,R}(t) = \sum_{t=1}^{T} \sum_{i=1}^{N} \Phi_i^d(t) \tag{57}$$

where $L_{heat,R}(t)_{ij}$ represents the heat load after demand response; $L_{BH}(t)$ represents the base heat load; $L_{MH}(t)$ represents the reducible heat load, which can be reduced by a certain proportion based on the actual energy usage of consumers; $L_{MH,max}$, $L_{MH,max}$ represent

upper and lower limits of reducible heat load; (57) is also used to describe load balance before and after demand response during one period.

3. The Solution of the Robust Bilevel Optimization Model

We focus on using the method of robust optimization to solve the bilevel optimization problem affected by data uncertainty [34]. The robust bilevel model can be expressed in Figure 1.

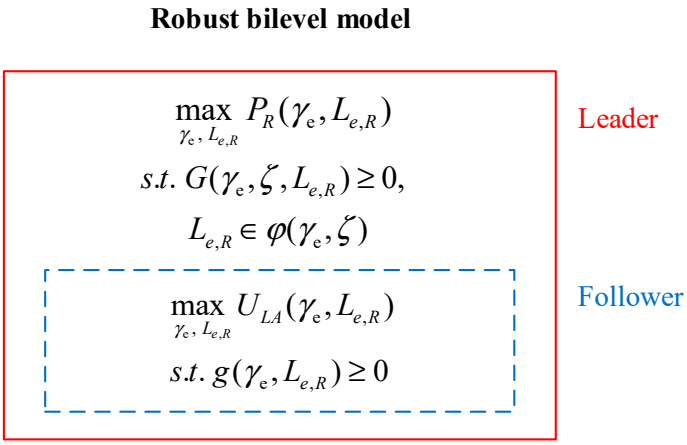


Figure 1. The robust bilevel model.

In the figure, $P_R(\gamma_e, L_{e,R})_{ij}$ denote the upper-level objective function (9); $U_{LA}(\gamma_e, L_{e,R})_{ij}$ represent the lower-level objective function (50); the upper-level constraints (11)–(49) are given by $G(\gamma_e, \zeta, L_{e,R}) \geq 0_{ij}$ that contain uncertain constraints (2)–(8); $g(\gamma_e, L_{e,R}) \geq 0_{ij}$ represents the lower-level constraints (52)–(57); $\varphi(\gamma_e, \zeta)$ is the set of optimal solutions of the (γ_e, ζ)-parameterized problem.

$$\varphi(\gamma_e, \zeta) := \underset{L_{e,R}*}{\operatorname{argmax}} \left\{ \min_{\zeta \in \Omega} U_{LA}(\gamma_e, \zeta, L_{e,R}*) : g(\gamma_e, \zeta, L_{e,R}*) \geq 0 \right\} \tag{58}$$

Note, that if adopting a sequential decision-making approach, the leader first will make a decision γ_e* that includes uncertain parameters, that is, without knowing the realization of uncertainty; Then, the follower will take a "wait-and-see" approach and make its decision $L_{e,R}*$ considering the leader's decision. The decision-making process implies that the leader may fail to understand the lower-level problem sufficiently due to the influence of uncertainty. Therefore, to hedge against the worst reactions of the follower, the leader needs not only to enhance robustness but also to overcome their conservatism in working with the follower. In summary, this sequential decision-making approach brings many inconveniences to solving robust bilevel optimization problems with uncertainty.

Based on the above analysis, as a nonlinear optimization problem, robust bilevel optimization can also be transformed into a single-level optimization problem of the Mathematical program with equilibrium constraints (MPEC) by utilizing the Karush–Kuhn–Tucker (KKT) conditions to construct the Lagrangian function of the original model [35]. The robust model and the transformed lower-level problem are solved together as constraints in the MPEC, which can significantly reduce the difficulty and complexity of the solution. In addition, it should be noted that the transformation of the lower-level model is subject to

certain conditions. Fortunately, both the objective function and constraints of the consumer model are convex and satisfy the Slater conditions [36].

$$\begin{gathered} \max_{\gamma_e,\, L_{e,R}} P_R(\gamma_e, L_{e,R}) \\ s.t.\ G(\gamma_e, \zeta, L_{e,R}) \geq 0, \\ \nabla_{L_{e,R}} U_{LA}(\gamma_e, L_{e,R}) + \lambda^\top \nabla_{L_{e,R}} g(\gamma_e, L_{e,R}) = 0, \\ g(\gamma_e, L_{e,R}) \geq 0,\ \lambda \geq 0, \\ \lambda^\top g(\gamma_e, L_{e,R}) = 0, \\ U_{LA}(\gamma_e, L_{e,R}) - \varphi(\gamma_e, \zeta)\ \leq 0 \end{gathered} \tag{59}$$

where λ is Lagrange multiplier vectors for constraints, respectively. The constraints are further linearized using the Big-M method [37]:

$$\begin{gathered} g(\gamma_e, L_{e,R}) \geq 0,\ \lambda \geq 0, \\ \lambda^\top g(\gamma_e, L_{e,R}) = 0 \end{gathered} \Leftrightarrow \begin{cases} g(\gamma_e, L_{e,R}) \leq Mz, \\ \lambda \leq M(1-z) \end{cases} \tag{60}$$

Within this transformation, a vector z composed of binary variables and a sufficiently large number M are introduced [38]. The Big-M method can further convert the MPEC model into a mixed-integer linear programming problem (MILP) problem, and the solution techniques for MILP are mature and stable.

4. Empirical Analysis

The simulation model of this paper is programmed by JuliaPro 1.5.4-1 [39] and solved by Gurobi 9.1.2 [40] software package.

4.1. Description of the Simulation System

4.1.1. PIES Topology

The system's topology in this chapter is shown in Figure 2. The PIES consists of a radial power network with 14 nodes [41], a heating network with 11 nodes [42], and a natural gas pipeline network with 6 nodes [43]. The base voltage of the radial power network is 10 kV, with a base power of 0.3 MW. Of the 14 nodes, three are power source nodes located at nodes 1, 2, and 6. Among them, Node 2 is equipped with wind turbine (WT), photovoltaic (PV), and energy storage (ES). Node 6 is connected to node 2 of the heating network through the CHP device, with the gas supplied by node 1 of the gas network. This power node is also coupled to a gas turbine (GT). Meanwhile, PIES has signed a power purchase and sale agreement with the power company, and interacts with the main network through node 1. The heating system of PIES is also radial, with a load level of 0.1 MW. Furthermore, the heating network is also equipped with three heat sources. It is known that node 2 is connected to a CHP unit, while the other heat sources are located at nodes 1 and 6; they are connected to gas boilers and node 3 of the gas network.

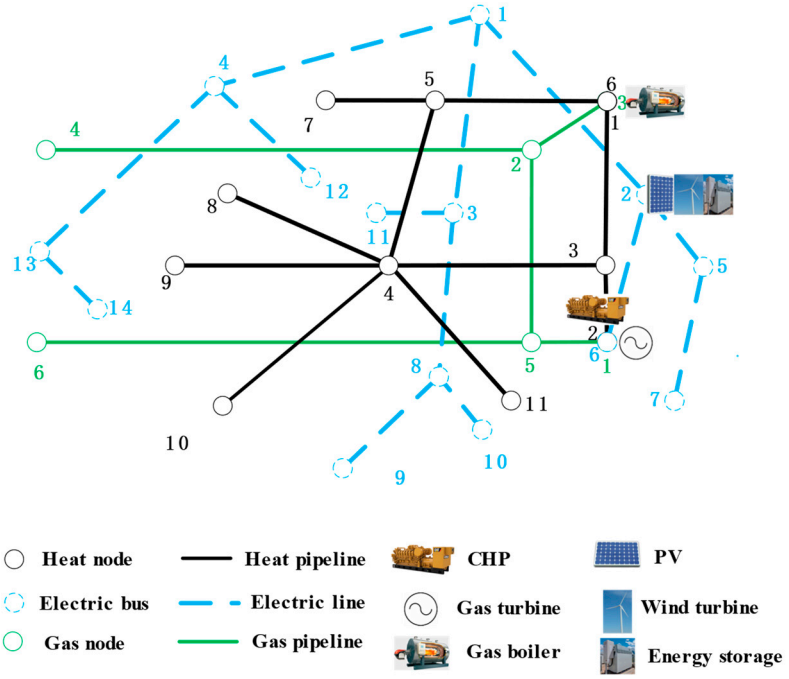


Figure 2. The topology of PIES.

4.1.2. Relevant Data and Model Parameters

Table 1 lists the device parameters involved in this paper.

Table 1. Key parameters of equipment in PIES.

Equipment	Parameters	Values
CHP	Heat-Electricity Ratio z_{CHP}	1.25
	Electrical efficiency η_{CHP}	0.25
Gas tur-bine	Gas calorific value H_g	39 MJ/m^3
	Electrical efficiency η_{GT}	0.55
Gas boiler	Thermal efficiency η_{GB}	0.92
Storage device	The upper limit of the capacity $E_{\max}$	0.5 MWh
	The lower limit of the capacity $E_{\min}$	0.05 MWh
	The upper limit of absorbing energy $P^{ch}_{\max}$	80 kW
	The lower limit of absorbing energy $P^{ch}_{\min}$	0 kW
	The upper limit of releasing energy $P^{ch}_{\max}$	125 kW
	The lower limit of releasing energy $P^{dis}_{\min}$	0 kW

Since the current load forecasting technology is quite mature, the power deviation of load forecasting in engineering applications can be controlled within 5 percentage points. Therefore, this paper no longer considers load uncertainty, and selects a typical daily load demand of a group of park users during simulation, as shown in Figure 3, including electrical load and thermal load curves.

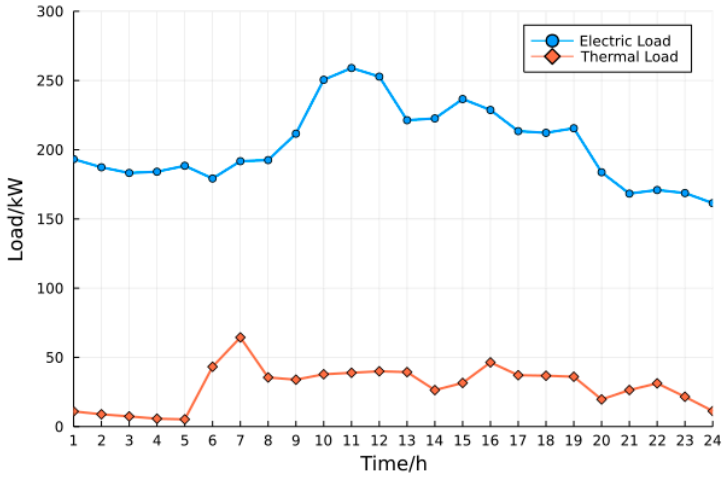


Figure 3. The typical daily load demand of consumers.

The price of time-sharing energy is shown in Table 2, which includes electricity price interaction with the power companies and the price of gas input to the PIES. The upper limit and lower limit of the interaction power are 60 kW and 50 kW, respectively.

Table 2. Time-sharing price of energy.

Period	Gas Price/Yuan	Interaction Price with Distribution Network/Yuan
1:00—7:00	3.5	0.41
8:00—10:00, 23:00—24:00	5.5	0.74
11:00—22:00	6.8	1.1

4.2. Simulation Results

The uncertainty of the robust optimization proposed in this paper is set to $W = 0.3$, minimize the deviation cost of the output of the renewable energy unit. It ensures that all the numbers around the predicted value can be covered under this uncertainty. The simulation results obtained by calculation are as follows:

Figure 4 shows the final confirmed sales pricing to consumers, which is lower than the energy prices outside of PIES.

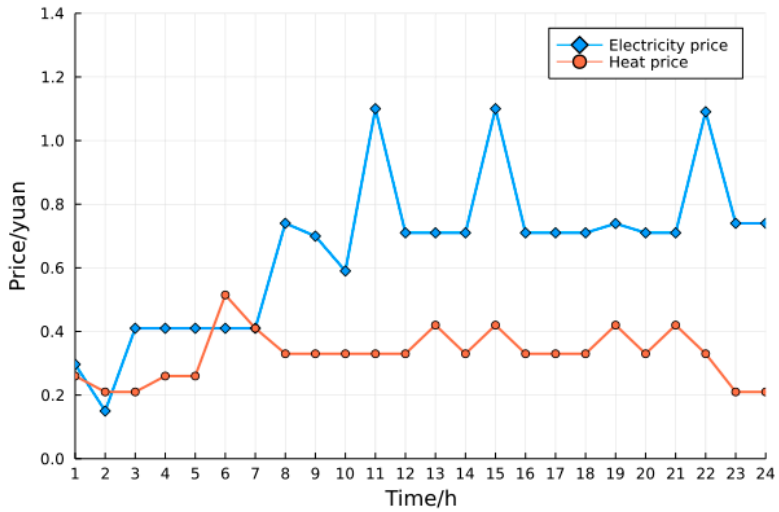


Figure 4. The price of purchasing electricity and heat by consumers from the operator.

As depicted in Figure 5, for the sake of the lowest natural gas prices observed from 1:00 to 7:00, the CHP and steam turbines focus on operating with high efficiency during this period, which can significantly reduce the operational costs of PIES. Furthermore, wind turbines generate more electricity while the corresponding power demand is relatively low. As a result, the energy storage device works in the charging state. From 7:00 to 19:00, photovoltaic and wind power output shows a complementary trend, but more than solely relying on renewable energy sources is needed to meet the high daytime power demand. Consequently, the operator purchases electricity from the power company. During the peak demand period at noon, energy storage devices discharge electricity, which can minimize the amount of purchased electricity at a high price. From 20:00 to 24:00, electricity demand decreases, and the PIES exports excess electricity to the outside. On the other hand, during the period from 7:00 to 24:00, natural gas prices remain relatively high. Because of the coupling relationship with the heating network, the CHP will maintain a basic output to meet the corresponding heat demand. In contrast, the gas turbine attempts to reduce the output during this period.

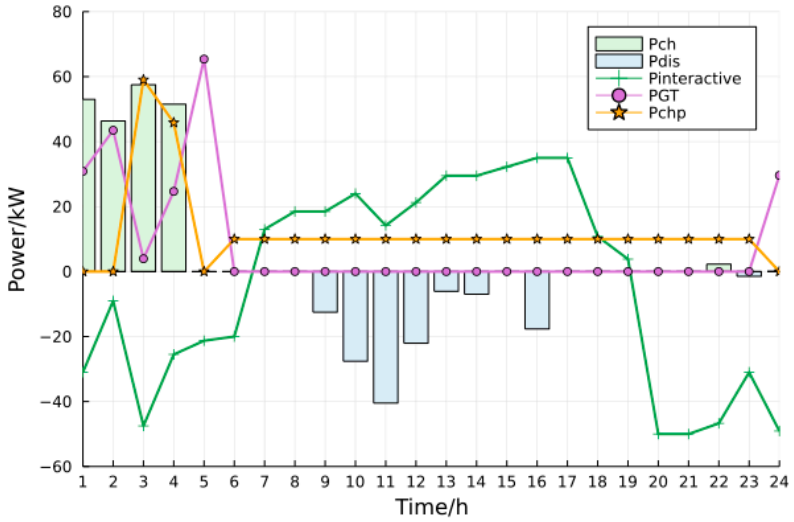


Figure 5. Optimization results of electrical power output.

As shown in Figure 6, the heating device provides heat energy according to the requirements of thermal consumers. The output of the boiler from 5:00 to 24:00 generally matches the energy consumption habits of consumers and ensures the fulfillment of most of the heating demand. As an electricity-heat coupling device, the CHP needs to consider both electric and thermal load demands. It can independently undertake the heating task when the heat load is low during 3:00–4:00 in the morning. From 6:00 to 23:00, it will maintain a basic heat output to meet the heat demand.

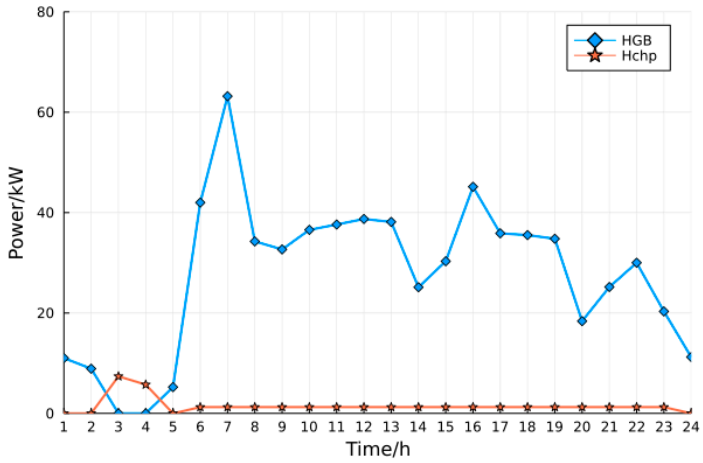


Figure 6. Optimization results of heat power output.

4.3. Case Studies

To verify the superiority of the PIES model proposed in this article, the following case studies are designed to conduct comparative analyses.

Case 1: PIES with robust bilevel optimization and multi-energy flow calculations.

Case 2: PIES without the bilevel optimization, nor consider the demand response of consumers.

Case 3: PIES without the multi-energy flow calculation.

Based on the above case, through optimization calculation, the revenue obtained by the operator from selling energy to consumers, the surplus of purchasing and selling electricity to the main network, and the cost of using gas can be obtained. The specific results obtained from the four cases are shown in the Table 3.

Table 3. The income comparison of PIES under different scenarios.

Case	Total Profit/Yuan	Revenue from Electricity Sales/Yuan	Revenue from Thermal Sales/Yuan	Operating Cost/Yuan	Interaction Cost/Yuan
1	46,978.81	32,674.56	26,437.56	12,142.88	−9.57
2	44,216.74	32,863.86	27,653.01	16,308.92	−8.79
3	47,388.26	32,674.56	26,437.56	11,316.00	−27.17

Compared with case 2, case 1 reduces the consumers' energy cost by 1404.75 yuan and increases the operator's total profit by 2674.21 yuan. Among them, a reduction of 189.3 yuan and 1215.45 yuan in the consumers' electricity and heating costs, respectively. The decrease in energy costs will inevitably lead to improved consumer satisfaction. On the other hand, although the revenue from selling energy to the operator decreased, the operating cost decreased even more, reaching 4166.04 yuan (the surplus from external electricity sales has not changed much, with only an additional revenue of 0.78 yuan). Therefore, the total profit has increased.

In addition, since Case 1 also considers consumers' demand response, a comparative analysis can be conducted by comparing the load variation charts before and after participating in the demand response.

Figure 7 shows that the fluctuation of electric load slows down significantly after participating in demand response. The load peaks during 10:00–12:00 and 14:00–17:00 are reduced, and the load valley during 20:00–24:00 is slightly lifted.

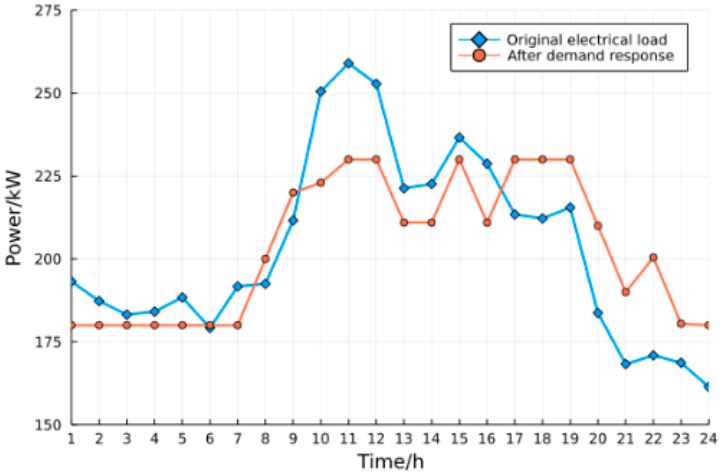


Figure 7. Comparison of electrical load before and after demand response.

Figure 8 illustrates the changes in the heat load before and after consumers participate in demand response. It can be observed that the peak-shaving and valley-filling effect of demand response is evident. The curve is slightly lifted when the heat demand is low from 1:00–6:00 in the morning. The peak heat demand at 7:00 is significantly reduced, and the fluctuation of the heat load curve in the subsequent period tends to be gentle. The above results show that the introduction of demand response and the game interaction between operators and consumers can not only reduce the energy cost of users and improve the comprehensive benefits of users, but also significantly improve the operation economy of PIES.

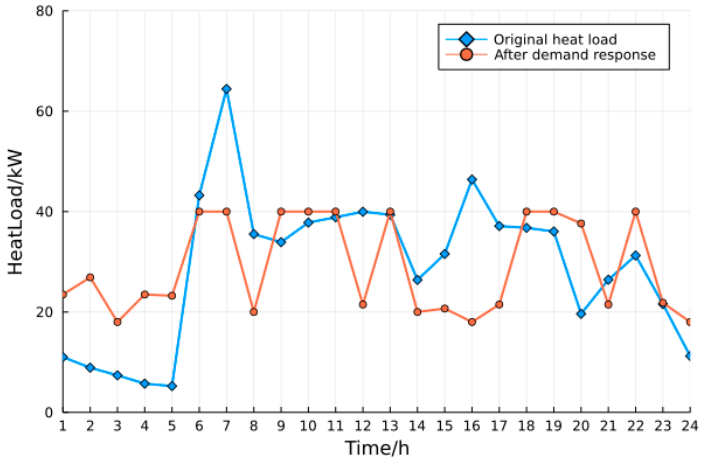


Figure 8. Comparison of heat load before and after demand response.

Since Case 3 does not consider the topology of PIES, there is no multi-energy flow constraint during operation optimization. Under the same load demand, the total profit of the operator is increased by 895.6 yuan compared with Case 1. Among them, the operating cost has been significantly reduced to 826.88 yuan. However, to measure the impact of multi-energy flow constraints on the system, in addition to considering the economy, also to measure the safety. To better illustrate the safety impact, the power (in per-unit values) of some power lines in the electrical network during the maximum electric load at 11:00 and the flow rate (in per-unit values) of some pipelines in the heating network during the maximum heat load at 7:00 are selected and displayed in Table 4.

Table 4. Partial line power and pipeline flux.

Case	Line Power/p.u.				
	1–2	**1–3**	**1–4**	**2–5**	**2–6**
1	0.756	0.425	0.684	0.129	0.840
3	**1.527**	0.762	1.01	0.156	**1.667**
Case	**Pipeline Flux/p.u.**				
	1–3	**2–3**	**3–4**	**6–5**	
1	0.452	0.467	0.919	0.893	
3	0.667	0.792	**1.459**	**1.144**	

As shown in the table, the power of the network lines and the flux of the thermal network pipelines in Case 1 are within a reasonable operating range, while in Case 3, the power limit is exceeded in the lines between nodes 1–2 and 2–6 of the power network, and the flux limit is exceeded in the pipelines between nodes 3–4 and 6–5 of the thermal network (data exceeding the baseline are shown in bold). Through the above results, the multi-energy flow calculation essentially considers the line or pipeline loss during the actual operation of the system. If the influence is ignored, it will lead to line overload or pipeline flow exceeding the limit. When the situation is serious, it may even cause unnecessary losses.

4.3.1. Comparison of Models in Sample

To verify the compactness of different sets, this paper compares the worst-case scenarios of the three set constraint ranges under various uncertainties, with the predicted value as the benchmark. The compactness of the set is defined as the parameter C_p to characterize.

$$C_p = \frac{|\Xi_{pre} - \Xi_i|}{\Xi_{pre}} \times 100\% \tag{61}$$

where Ξ_i is the upper limit of the coverage area of set i, and Ξ_{pre} is the predicted value. When comparing under the same uncertainty, i represents the box set, ellipsoidal set, and ellipsoidal set proposed in this paper, respectively.

(1) Box set [44]:

$$\Omega = \{\zeta : |\zeta| \leq 1, \zeta \leq W\} \tag{62}$$

where ζ is the interval scheduling coefficient; $u_{error}^{\max}$ is the maximum prediction error; $\overline{u}$ is the predicted value, and the uncertainty interval of the parameter is $[\overline{u} - \zeta u_{error}^{\max}, \overline{u} + \zeta u_{error}^{\max}]$.

(2) Ellipsoid Set [45]:

$$\Omega = \left\{u \in R^{n_u} : (u - \overline{u}) \sum\nolimits_1 (u - \overline{u}) \leq W\right\} \tag{63}$$

where u is the uncertain argument; Σ_1 is a covariance matrix.

The set with a smaller C_p value indicates a more compact set with a weaker conservatism of the corresponding robust optimization model. When analyzing within the same set, the change in the value of C_p with the increase in uncertainty W indicates the trend of the coverage area of the set.

The comparison results are shown in Figure 9:

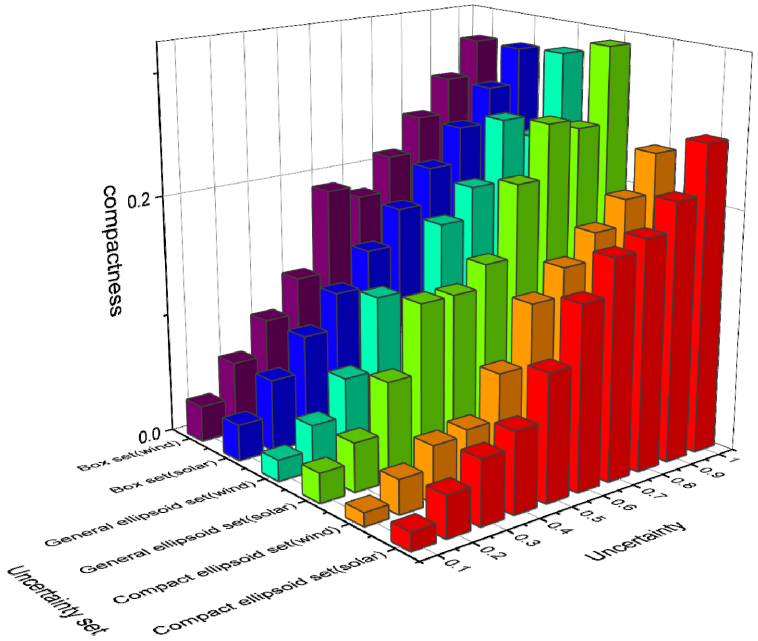


Figure 9. Comparison of compactness among different uncertainty sets.

At the same level of uncertainty, the C_p values of the ellipsoidal set proposed in this paper are smaller than those of the box set and the general ellipsoidal set, indicating that the compactness of the set is superior to the compared sets, making the resulting solutions of the robust optimization model less conservative. With the increase in uncertainty, the C_p values of the box set and the proposed set are both monotonically increasing, but the range of variation of the proposed set is smaller than that of the box set. Although the C_p value of the general ellipsoidal set shows an increasing trend, there are fluctuations before and after. The rising C_p values indicate that the coverage area of the set gradually expands with the increase in uncertainty, which is beneficial for adjusting the constraint range of renewable energy unit output more finely. The fluctuation of the C_p value for a general ellipsoid set makes it not conducive to changing the tightness of the set by adjusting the uncertainty. In comparison, the proposed ellipsoid set not only has a higher tightness than other sets but also has a smaller range of adjustability and a more obvious regularity in adjustability.

4.3.2. Comparison of Models under Out-of-Sample Simulation

The following compares the compactness of the three uncertain sets in the simulation outside the sample. The concept of "out-of-sample" corresponds to "in-sample". The "in-sample" data refers to the historical data of wind and solar used in the robust model proposed in this paper, while the "out-of-sample" data are to regenerate 3000 sets of wind and solar active power output data that conform to the normal distribution through the Monte Carlo method to verify the economy and safety of the robust model using different uncertainty sets. The process of security verification includes setting the decision variable of the scheduling strategy as a fixed value, inputting 3000 sets of wind and light data into the robust model represented by three uncertain sets, and using the power flow convergence rate as the evaluation standard to verify the power flow convergence state of the system. The methodology for calculating the power flow convergence rate R is as follows:

$$\mathrm{R} = \frac{N_C}{3000} \times 100\% \tag{64}$$

where N_C represents the number of wind and solar data sets that can make the power flow convergence.

Based on Table 5, it can be observed that the ellipsoid set model proposed in this paper approaches is close to complete convergence when the uncertainty is 0.2, while the box

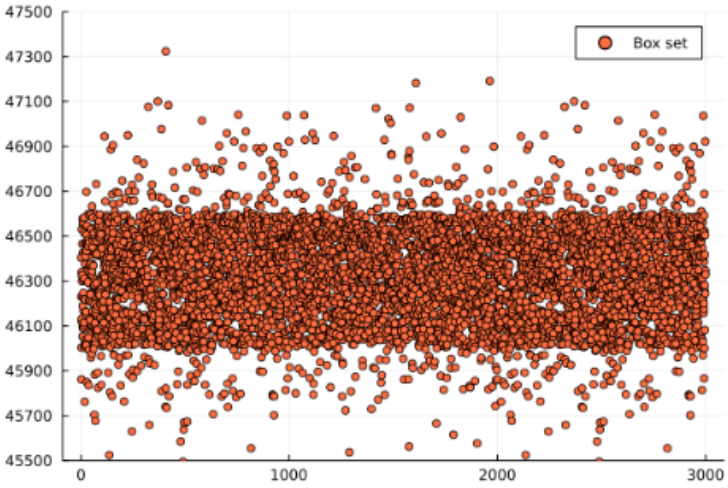
set and general ellipsoidal set only achieve full convergence after the uncertainty reaches 0.4 and 0.6, respectively. The proposed ellipsoid set ensures power flow convergence by comparing the convergence rates. The solutions obtained from the ellipsoid set are more compact, and robust, and the power flow convergence is better than the other two sets.

Table 5. Comparison of the convergence rate of power flow in different sets.

Uncertainty	Box Set	General Ellipsoid Set	Compact Ellipsoid Set
$W = 0.1$	97.32%	96.51%	98.45%
$W = 0.2$	98.67%	97.18%	99.99%
$W = 0.3$	99.28%	96.98%	100%
$W = 0.4$	100%	98.79%	100%
$W = 0.5$	100%	99.02%	100%
$W = 0.6$	100%	100%	100%
$W = 0.7$	100%	100%	100%
$W = 0.8$	100%	100%	100%
$W = 0.9$	100%	100%	100%
$W = 1$	100%	100%	100%

When comparing economics, it is known that the three robust models can converge when the uncertainty is 0.6. Under this condition, according to the dispatch strategy proposed in case 1, the operator's profit after three different robust optimizations are calculated, respectively. Figure 10 shows the scatter plot of the resulting profit.

From Figure 10 scatter plot and Table 6, it can be observed that the proposed ellipsoidal set has the highest expected value, and its scatter plot is more condensed. Using the box set provides the lowest expected value, and the scatter plot has the highest root mean square. In the scatter plot using a general ellipsoid set, the data sparsity is between the above two sets. Therefore, the proposed ellipsoidal set robust optimization model has superior compactness with better robustness and lower conservatism, making it advantageous over the box set and general ellipsoidal set in improving the operational economy of the system.



(**a**)

Figure 10. *Cont.*

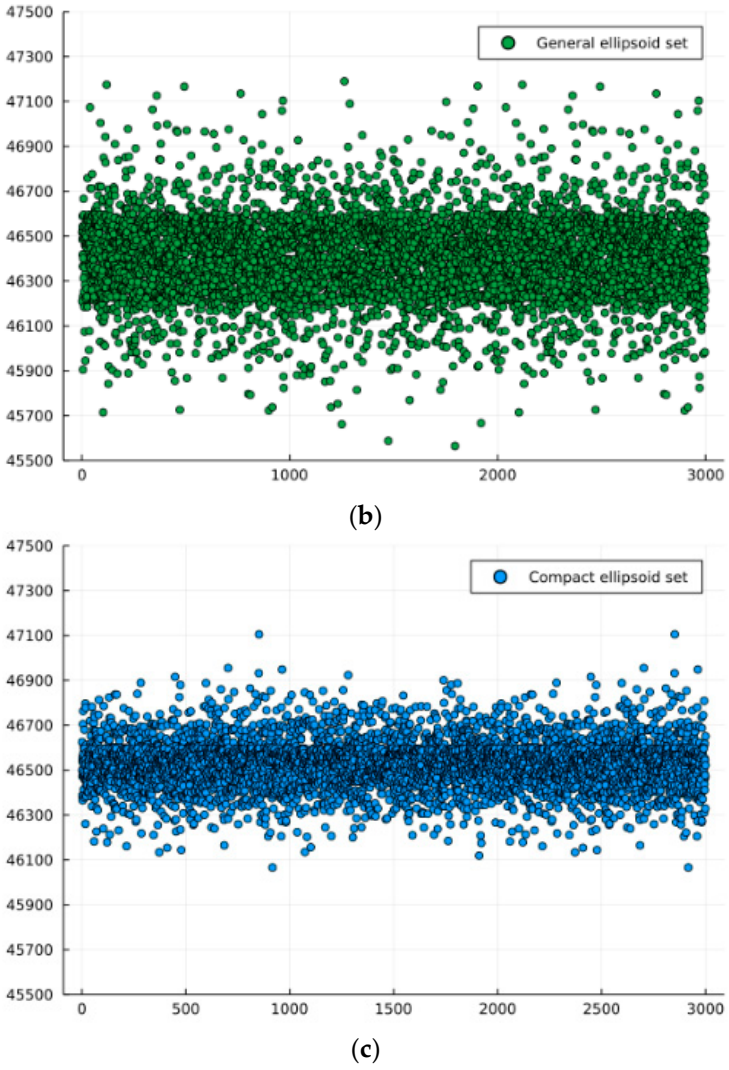


Figure 10. Comparison of the operator's profit under different sets. (**a**) The profit obtained by operator using the box set. (**b**) The profit obtained by operator using the general ellipsoid set. (**c**) The profit obtained by operator using the proposed set.

Table 6. Expected values and mean root square of operator's profit.

Uncertainty Set	Expected Values/Yuan	Root Mean Square/Yuan
Box set	46,305.98	210.44
General ellipsoid set	46,401.58	187.75
Proposed ellipsoid set	46,522.61	98.24

5. Conclusions and Future Work

5.1. Conclusions

This paper constructs a robust uncertainty set based on the K-means++ algorithm to deal with the uncertainty of renewable energy output. Then, the robust bi-level dispatch strategy is proposed, with the operator as the leader and consumers as the follower. Optimizing the pricing strategies of energy sources to determine the output of each energy conversion equipment and the demand response plan to achieve cooperative and interactive operation between subjects. Finally, case studies have fully demonstrated the effectiveness and practicality of the proposed dispatch model. The following conclusions are as follows:

(1) The robust optimization model based on the K-means++ clustering algorithm has high compactness, strong robustness, and low conservatism under in-sample and out-of-sample simulation.

(2) Case studies show that the proposed optimization strategy can significantly reduce the operating cost and improve the operation economy of PIES.

(3) After the introduction of demand response and bi-level optimization mechanism, the load fluctuations slow down, and the effect of lowering peak-valley differences is noticeable while enhancing the system's safety and stability. In addition, for consumers, the energy consumption cost is reduced, and the satisfaction of energy consumption is improved.

5.2. Future Work

There are still some considerations for further study.

The research content will introduce the energy price game between PIES and external power companies or natural gas companies. In addition, the research background can also be expanded to the multi-operator interest interaction in multi-integrated energy systems, and more complex income distribution strategies can be explored.

Author Contributions: Conceptualization, P.W. and X.B.; methodology, P.W., L.Z. and X.B.; software, P.W., L.Z. and X.B.; validation, P.W.; formal analysis, P.W.; investigation, P.W.; resources, P.W.; data curation, P.W., L.Z. and T.D.; writing—original draft preparation, P.W.; writing—review and editing, L.Z., T.D., S.H. and X.B.; visualization, P.W. and L.Z.; supervision, P.W. and X.B.; project administration, P.W. and X.B.; funding acquisition, P.W. and X.B. All authors have read and agreed to the published version of the manuscript.

Funding: This research was funded by the National Natural Science Foundation of China (Grant no. 51967001) and Innovation Project of Guangxi Graduate Education (Grant no. YCSW2023063).

Data Availability Statement: Not applicable.

Conflicts of Interest: The authors declare no conflict of interest.

References

1. Gao, C.; Zhang, Z.; Wang, P. Day-Ahead Scheduling Strategy Optimization of Electric–Thermal Integrated Energy System to Improve the Proportion of New Energy. *Energies* **2023**, *16*, 3781. [CrossRef]
2. Xu, G.; Dong, H.; Xu, Z.; Bhattarai, N. China can reach carbon neutrality before 2050 by improving economic development quality. *Energy* **2022**, *243*, 123087. [CrossRef]
3. Wang, L.; Lin, J.; Dong, H.; Wang, Y.; Zeng, M. Demand response comprehensive incentive mechanism-based multi-time scale optimization scheduling for park integrated energy system. *Energy* **2023**, *270*, 126893. [CrossRef]
4. Xu, Q.; Li, L.; Chen, X.; Huang, Y.; Luan, K.; Yang, B. Optimal economic dispatch of combined cooling, heating and power-Type multimicrogrids considering interaction power among microgrids. *IET Smart Grid* **2019**, *2*, 391–398. [CrossRef]
5. Tan, Z.; Yang, S.; Lin, H.; De, G.; Ju, L.; Zhou, F. Multi-scenario operation optimization model for park integrated energy system based on multi-energy demand response. *Sustain. Cities Soc.* **2019**, *53*, 101973. [CrossRef]
6. Ben-Tal, A.; Ghaoui, L.; Nemirovski, A. *Robust Optimization*; Princeton University Press: Princeton, NJ, USA, 2009.
7. Bertsimas, D.; Brown, D.B.; Caramanis, C. Theory and Applications of Robust Optimization. *SIAM Rev.* **2011**, *53*, 464–501. [CrossRef]
8. Chen, F.; Deng, H.; Chen, Y.; Wang, J.; Jiang, C.; Shao, Z. Distributed robust cooperative scheduling of multi-region integrated energy system considering dynamic characteristics of networks. *Int. J. Electr. Power Energy Syst.* **2023**, *145*, 108605. [CrossRef]
9. Kuryatnikova, O.; Ghaddar, B.; Molzahn, D.K. Adjustable Robust Two-Stage Polynomial Optimization with Application to AC Optimal Power Flow. *arXiv* **2021**, arXiv:2104.03107.
10. Shang, C.; You, F. A data-driven robust optimization approach to scenario-based stochastic model predictive control. *J. Process. Control* **2019**, *75*, 24–39. [CrossRef]
11. Li, F.; Su, J.; Sun, B. An Optimal Scheduling Method for an Integrated Energy System Based on an Improved k-Means Clustering Algorithm. *Energies* **2023**, *16*, 3713. [CrossRef]
12. Massrur, H.R.; Niknam, T.; Fotuhi-Firuzabad, M. Investigation of Carrier Demand Response Uncertainty on Energy Flow of Renewable-Based Integrated Electricity–Gas–Heat Systems. *IEEE Trans. Ind. Informatics* **2018**, *14*, 5133–5142. [CrossRef]
13. Taheri, B.; Jabari, F.; Foroud, A.A. A green cogeneration microgrid composed of water-source heat pumps, a gravity energy storage, and a bio-fueled gas turbine: Design and techno-economic optimization. *Sustain. Cities Soc.* **2023**, *95*, 104594. [CrossRef]

14. Pastore, L.M. Combining Power-to-Heat and Power-to-Vehicle strategies to provide system flexibility in smart urban energy districts. *Sustain. Cities Soc.* **2023**, *94*, 104548. [CrossRef]
15. Lu, Q.; Guo, Q.; Zeng, W. Optimal dispatch of community integrated energy system based on Stackelberg game and integrated demand response under carbon trading mechanism. *Appl. Therm. Eng.* **2023**, *219*, 119508. [CrossRef]
16. Liu, Z.; Li, C. Low-Carbon Economic Optimization of Integrated Energy System Considering Refined Utilization of Hydrogen Energy and Generalized Energy Storage. *Energies* **2023**, *16*, 5700. [CrossRef]
17. Kong, D.; Jing, J.; Gu, T.; Wei, X.; Sa, X.; Yang, Y.; Zhang, Z. Theoretical Analysis of Integrated Community Energy Systems (ICES) Considering Integrated Demand Response (IDR): A Review of the System Modelling and Optimization. *Energies* **2023**, *16*, 4129. [CrossRef]
18. De, G.; Wang, X.; Tian, X.; Xu, T.; Tan, Z. A Collaborative Optimization Model for Integrated Energy System Considering Multi-Load Demand Response. *Energies* **2022**, *15*, 2033. [CrossRef]
19. Zheng, W.; Lu, H.; Zhang, M.; Wu, Q.; Hou, Y.; Zhu, J. Distributed Energy Management of Multi-Entity Integrated Electricity and Heat Systems: A Review of Architectures, Optimization Algorithms, and Prospects. *IEEE Trans. Smart Grid* **2023**. *Early Access*. [CrossRef]
20. Singh, M.K.; Kekatos, V. Natural Gas Flow Solvers Using Convex Relaxation. *IEEE Trans. Control Netw. Syst.* **2020**, *7*, 1283–1295. [CrossRef]
21. Ding, J.; Gao, C.; Song, M.; Yan, X.; Chen, T. Optimal operation of multi-agent electricity-heat-hydrogen sharing in integrated energy system based on Nash bargaining. *Int. J. Electr. Power Energy Syst.* **2023**, *148*, 108930. [CrossRef]
22. Yang, S.; Tan, Z.; Zhou, J.; Xue, F.; Gao, H.; Lin, H.; Zhou, F. A two-level game optimal dispatching model for the park integrated energy system considering Stackelberg and cooperative games. *Int. J. Electr. Power Energy Syst.* **2021**, *130*, 106959. [CrossRef]
23. Qin, X.; Sun, H.; Shen, X.; Guo, Y.; Guo, Q.; Xia, T. A generalized quasi-dynamic model for electric-heat coupling integrated energy system with distributed energy resources. *Appl. Energy* **2019**, *251*, 113270. [CrossRef]
24. Wang, S.; Wu, Z.; Zhuang, J. Optimal Dispatching Model of CCHP Type Regional Multi-microgrids Considering Interactive Power Exchange Among Microgrids and Output Coordination Among Micro-sources. *Zhongguo Dianji Gongcheng Xuebao/Proc. Chin. Soc. Electr. Eng.* **2017**, *37*, 7185–7194.
25. Beck, Y.; Ljubić, I.; Schmidt, M. A survey on bilevel optimization under uncertainty. *Eur. J. Oper. Res.* **2023**, *311*, 401–426. [CrossRef]
26. Nasiri, N.; Zeynali, S.; Ravadanegh, S.N. A tactical transactive energy scheduling for the electric vehicle-integrated networked microgrids. *Sustain. Cities Soc.* **2022**, *83*, 103943. [CrossRef]
27. Burtscheidt, J.; Claus, M. Bilevel Linear Optimization Under Uncertainty. In *Bilevel Optimization: Advances and Next Challenges*; Dempe, S., Zemkoho, A., Eds.; Springer International Publishing: Cham, Switzerland, 2020; pp. 485–511.
28. Wu, Y.; Yao, L.; Liao, S.; Liu, Y.; Li, J.; Wang, X. A Peak Shaving Method of Aggregating the Distributed Photovoltaics and Energy Storages Based on the Improved K-means++ Algorithm. *Dianwang Jishu/Power Syst. Technol.* **2022**, *46*, 3923–3931.
29. Zhao, S.; Yao, J.; Li, Z. Wind Power Scenario Reduction Based on Improved K-means Clustering and SBR Algorithm. *Dianwang Jishu/Power Syst. Technol.* **2021**, *45*, 3947–3954.
30. Kocuk, B.; Dey, S.S.; Andy Sun, X. Strong SOCP relaxations for the optimal power flow problem. *Oper. Res.* **2016**, *64*, 1177–1196. [CrossRef]
31. Li, P.; Wu, D.; Li, Y.; Liu, H.; Wang, N.; Zhou, X. Optimal Dispatch of Multi-microgrids Integrated Energy System Based on Integrated Demand Response and Stackelberg game. *Zhongguo Dianji Gongcheng Xuebao/Proc. Chin. Soc. Electr. Eng.* **2021**, *41*, 1307–1321.
32. Chai, B.; Chen, J.; Yang, Z.; Zhang, Y. Demand Response Management with Multiple Utility Companies: A Two-Level Game Approach. *IEEE Trans. Smart Grid* **2014**, *5*, 722–731. [CrossRef]
33. Maharjan, S.; Zhu, Q.; Zhang, Y.; Gjessing, S.; Basar, T. Dependable Demand Response Management in the Smart Grid: A Stackelberg Game Approach. *IEEE Trans. Smart Grid* **2013**, *4*, 120–132. [CrossRef]
34. Beck, Y.; Schmidt, M. *A Gentle and Incomplete Introduction to Bilevel Optimization*; Trier University: Trier, Germany, 2021.
35. Beck, Y.; Schmidt, M. A Robust Approach for Modeling Limited Observability in Bilevel Optimization. *Oper. Res. Lett.* **2021**, *49*, 752–758. [CrossRef]
36. Beck, Y.; Ljubić, I.; Schmidt, M. A Brief Introduction to Robust Bilevel Optimization. *arXiv* **2022**, arXiv:2211.16072.
37. Pineda, S.; Morales, J.M. Solving Linear Bilevel Problems Using Big-Ms: Not All That Glitters Is Gold. *IEEE Trans. Power Syst.* **2019**, *34*, 2469–2471. [CrossRef]
38. Fortuny-Amat, J.; McCarl, B. A Representation and Economic Interpretation of a Two-Level Programming Problem. *J. Oper. Res. Soc.* **1981**, *32*, 783–792. [CrossRef]
39. Julia Computing, Inc. JuliaPro Documentation. 2022. Available online: https://juliacomputing.com/docs/ (accessed on 3 October 2023).
40. Gurobi Optimizer 9.1. Available online: http://www.gurobi.com (accessed on 3 October 2023).
41. Tian, Y.; Liao, Q.; Liu, D.; Zhu, Z.; Peng, S.; Xu, Y. Planning of urban distribution network considering the integrated energy supply-side reform. *Power Syst. Technol.* **2016**, *40*, 2924–2933.
42. Qin, X.; Shen, X.; Guo, Y.; Pan, Z.; Guo, Q.; Sun, H. Combined Electric and Heat System Testbeds for Power Flow Analysis and Economic Dispatch. *CSEE J. Power Energy Syst.* **2021**, *7*, 34–44. [CrossRef]

43. Zhou, X.; Bao, Y.Q.; Ji, T.; Wang, Q. Two-Layer Optimization Scheduling Model of Integrated Electricity and Natural Gas Energy System Considering the Feasibility of Gas-Fired Units' Reserve. *IEEE Access* **2020**, *8*, 40337–40346. [CrossRef]
44. Jiang, S.-L.; Peng, G.; Bogle, I.D.L.; Zheng, Z. Two-stage robust optimization approach for flexible oxygen distribution under uncertainty in integrated iron and steel plants. *Appl. Energy* **2022**, *306*, 118022. [CrossRef]
45. Sadat, S.A. Optimal Bidding Strategy for a Strategic Power Producer Using Mixed Integer Programming. Ph.D. Thesis, University of South Florida, Tampa, FL, USA, 2017.

Disclaimer/Publisher's Note: The statements, opinions and data contained in all publications are solely those of the individual author(s) and contributor(s) and not of MDPI and/or the editor(s). MDPI and/or the editor(s) disclaim responsibility for any injury to people or property resulting from any ideas, methods, instructions or products referred to in the content.